Realistic correction of sky-coloured points in Mobile Laser Scanning point clouds

González, Elena; Balado, Jesús; Arias, Pedro; Lorenzo, Henrique

DOI
10.1016/j.optlastec.2021.107807

Publication date
2022

Document Version
Final published version

Published in
Optics and Laser Technology

Optics & Laser Technology 149 (2022) 107807

Contents lists available at ScienceDirect

Optics and Laser Technology

journal homepage: www.elsevier.com/locate/optlastec

Realistic correction of sky-coloured points in Mobile Laser Scanning point clouds

Elena González [a], Jesús Balado [a,b,*], Pedro Arias [a], Henrique Lorenzo [a]

[a] CINTECX, Universidade de Vigo, GeoTECH Group, 36310 Vigo, Spain
[b] Faculty of Architecture and the Built Environment, Delft University of Technology, GIS Technology Section. 2628 BL Delft, the Netherlands

ARTICLE INFO

Keywords:
LiDAR
Point cloud processing
Image processing
Coloured point cloud
Mobile Mapping Systems
Lab colour space

ABSTRACT

The enrichment of the point clouds with colour images improves the visualisation of the data as well as the segmentation and recognition processes. Coloured point clouds are becoming increasingly common, however, the colour they display is not always as expected. Errors in the colouring of point clouds acquired with Mobile Laser Scanning are due to perspective in the camera image, different resolution or poor calibration between the LiDAR sensor and the image sensor. The consequences of these errors are noticeable in elements captured in images, but not in point clouds, such as the sky. This paper focuses on the correction of the sky-coloured points, without resorting to the images that were initially used to colour the whole point cloud. The proposed method consists of three stages. First the region of interest where the erroneously coloured points are accumulated, is selected. Second, the sky-coloured points are detected by calculating the colour distance in the Lab colour space to a sample of the sky-colour. And third, the colour of the sky-coloured detected points is restored from the colour of the nearby points. The method is tested in ten real case studies with their corresponding point clouds from urban and rural areas. In two case studies, sky-coloured points were assigned manually and the remaining eight case studies, the sky-coloured points are derived from the acquisition errors. The algorithm for sky-coloured points detection obtained an average *F1-score* of 94.7%. The results show a correct reassignment of colour, texture, and patterns, while improving the point cloud visualisation.

1. Introduction

In recent decades 3D point cloud captured through LIDAR (Light Detection and Ranging) have attracted the interest of many areas, for instance autonomous driving, intelligent transportation systems, land administration, robotics, urban environment, archaeology, and architecture, since it provides a fast way to acquire real world. In particular, MLS (Mobile Laser Scanner) technology provides an accurate dataset composed of Cartesian coordinates (x, y, z) along with light reflectivity [1], in which each point in the point cloud corresponds to a precise 3D location of the environment surfaces. Data captured by MLS must be processed in order to extract useful geometric, topologic and semantic information [2] from the unstructured point cloud, or to fusion the point cloud with another data source.

Regarding appropriate scene understanding, a common strategy uses RGB image captured by camera, as source of visual meaning to complete geometric information extracted from Mobile Mapping System (MMS) 3D point cloud [3–5]. To tie point – pixel, the relationship given by pinhole projective geometry is adopted [6]. Despite that relationship, in fact 3D point cloud and sensor image are independent sources of data treated with quite different technology and stored separately. 3D point cloud needs to be saved along with sensor images in order to extract meaning at any time, and to divert the processing from one to another source of information for different purposes introducing computational cost. A natural step forward from that strategy is to use colourised 3D point cloud in which the data for each point are Cartesian coordinates and RGB values [5,7].

Incorporating colour to 3D point cloud ensures a more complete and independent data and closer to real environment, which improves machine and human scene understanding. Beyond aesthetic purposes in realistic visualization, colourised 3D point cloud allows to apply own techniques on volumes or projections onto planes of interest, and to extend 2D techniques used in image to 3D point cloud for applications as feature extraction, object detection, and segmentation. Thus, techniques have been proposed using colour in 3D point cloud, alone or along with other properties and in different colour spaces, in own 3D point cloud

* Corresponding author at: CINTECX, Universidade de Vigo, GeoTECH Group, 36310 Vigo, Spain.
E-mail address: jbalado@uvigo.es (J. Balado).

https://doi.org/10.1016/j.optlastec.2021.107807
Received 1 December 2020; Received in revised form 13 September 2021; Accepted 15 December 2021
Available online 22 December 2021

approaches as well as extension of 2D technique for 3D. To cite some, Kang et al. [8] used colourised 3D point cloud for line feature extraction; Luo et al. [7] based on octrees for semantic labelling; authors in references [9,10] proposed segmentation approaches based on using colour along with geometry, extending 2D techniques to 3D, graph and clustering, respectively. Meanwhile, Ximin et al. [11] used only colour RGB space for segmentation; Zhan et al. [12] developed a technique based on the transformation from RGB space to HSV (Hue, Saturation, Value) space; Perdomo et al. [13] used jointly colour and shape, as well as in [14] who, in addition, considered CIELAB colour space.

A key aspect in colourised 3D point cloud, is that points have the correct colour. To this end, strict calibration procedures must be followed [15]. However, even with a correct calibration, the colouring can be wrong. The sensors position based on GNSS-IMU systems hold errors reflected in the point clouds and their correct colour. Another more seriously problem is the lack of biunivocal relationship between MLS 3D point cloud and sensor image, in other words, a different resolution, which means that more than one point correspond to the same pixel in the image, introducing mistakes in colouring. Several authors have paid attention to correction of colour in different areas. For instance, Hasan et al. [16] corrected colourised aerial LIDAR point clouds by applying the model coefficients, while Yilmaz and Hellwich [17] suggested a technique for colour balancing in reconstruction. Bohak et al. [18] generate points on the surface of the water and colour them with orthophotos. In addition, there is a growing activity in improving point cloud colouring through adding devices [19,20], including online [21] and offline solutions [22] with the aim of providing rendering to the 3D point cloud.

This paper focuses on analysing and correcting colour in colourised 3D point cloud with the aim of achieving an autonomous set of data to be stored, saved and processed independently of other information, avoiding the use of different means, such as images, improving precision, while computational storage and processing costs are reduced. In particular, this work highlights a notable gap in the relationship between MLS data and image: while the entire environment is captured by the camera, distant elements are not represented in MLS data. This fact has effect on the colouring of elements whose contour is adjacent to the sky, giving rise to 3D points that are erroneously coloured with sky colour. From the best of our knowledge few attentions have been paid to this problem and this approach has not been presented in literature. The technique proposed in this paper improves notably colorized 3D point cloud.

The reminder of this paper is structured as follows. The proposed method is explained in Section 2. Section 3 is dedicated to the analysis of the results. The discussion is in Section 4 and Section 5 concludes this paper.

2. Method

2.1. Problem definition

LiDAR technology does not acquire colour by means of laser scanning. To colour MLS point clouds, images with a camera must be acquired simultaneously with the LiDAR data. Both the camera and the laser sensor are connected to an GNSS-IMU, so location and orientation each picture shot is known [23]. The association of image colours to point clouds is performed by a projection image to point cloud based on the pinhole model [24]. Each point of the cloud is projected onto the image from the focal perspective of the camera, or the image is projected onto the point cloud. The points belonging to each pixel are coloured according to pixel RGB components. Projections are made by means of rotation-translation matrices, calibrated beforehand with the position of the camera regarding to the laser sensor [25,26]. The calibration has a direct influence on the quality of the colouring of the point cloud. Wrong colour assignment on the edges of adjacent objects are due to a poor calibration. Thus, the points projected on the pixels do not coincide with the same object. In the case of the sky, the aim of this work, the sky does not return LiDAR points, but sky is colourful in images, therefore when a mismatch occurs, edges points in sky-adjacent objects are assigned with sky colour (Fig. 1).

2.2. Overview and input data

The proposed method for the correction of sky-coloured points is composed of three stages: Region of Interest (ROI) delimitation, detection of the sky coloured points, and reassignment of the colour. Point clouds with colour information are used as input data P(P_x,P_y,P_z,P_R,P_G, P_B). Usually, other point cloud attributes (such as intensity, timestamp, scan angle, number of returns, etc.) and extra information (images to coloured the point cloud, trajectory, etc.) are not always available in some datasets, as that information could be discarded, lost or simply not delivered to the end user [27]. For these reasons, the proposed method minimizes the input information used, only including the XYZ coordinates (basic geometric information inherent to the point cloud) and the RGB colour of the points to be corrected. The pseudo-code of the proposed method is collected in the Algorithm 1.

Algorithm 1

Inputs: Coloured_Point_Cloud {P}, Sample_Sky {S}, threshold *d*, height_MLS *h*
Outputs: Corrected_Point_Cloud {C}
Ground_plane G ← MLESAC(P)
Points_without_ROI {nR}←{Ø}
Points_within_ROI {R}←{Ø}
For each P(i)
  If distance_point_plane (G, P_i) < *h*
    {nR} ← Add P_i
  Else
    {R} ← Add P_i
  End If
End For
Points_with_Lab_attributes {R_{Lab}} ← rgb_to_lab (R_{RGB})
Sample_with_Lab_attributes {S_{Lab}} ← rgb_to_lab (S_{RGB})
Points_sky_coloured {K}←{Ø}
Points_no-sky_coloured {nK}←{nR}
For each R(i)
  If distance_colors ($S_{ab,}$ R_{ab_i}) < *d*
    {K} ← Add R_i
  Else
{nK} ← Add R_i
End If
End For
Relation_nearest_points {id} ← knnsearch (K, nK, k = 25 neighbors)
For each K(i)
Points_nK_nearest_Ki {N} ← nK(id_i)
Distances_color_to_nearest_points {Dn} ← distance_colors ($N_{ab,}$ K_{ab_i})
K_{RGB} ← {N_{RGB}: Dn == max(Dn)}
End For
{C} ← K ∪ nK
Return {C}

2.3. Delimitation of the region of interest

The sky coloured points are located in high elements and in borders of sky-adjacent elements, in view from camera focal point. The objects presenting a greater number of sky-coloured points are corners of buildings (roof edges and wall edges), pole like objects, trees, cables, and chains. As common characteristic, elements with sky-coloured points are higher than the height of the MLS. The first step of the proposed method is to delimit the Region of Interest (ROI) where colouring errors are concentrated. As ROI, points with a height (Z-coordinate distance to the ground) greater than the MLS height are selected. There are two important advantages to delimiting the study area:

- False positives are reduced in areas close to the ground that may coincide with sky blue: posters, traffic signs, cars, etc.

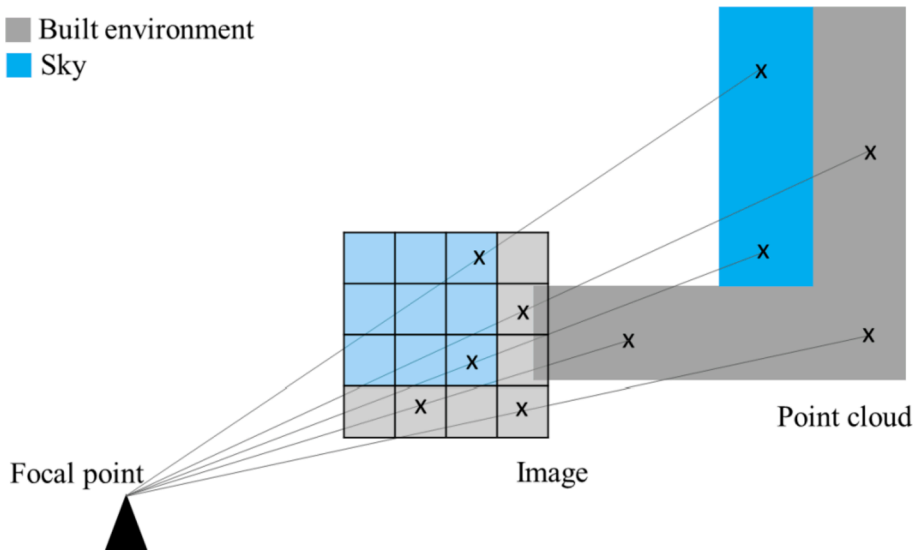

Fig. 1. Pinhole model. Projection with mismatch calibration from the pixels in the image (containing sky and built environment) to the point cloud (containing only built environment), resulting in part of the point cloud erroneously being coloured with sky.

- Processing time is reduced. The roads under MLS acquisition concentrates most of the points of the cloud. Eliminating ground points considerably reduces the processing time of the rest of the operations by reducing the number of points.

There are several ways to segment the point cloud by height [28]. A direct solution is, given the scan angle attribute, to select those points whose angles correspond to the ground orientation [29]. However, as mentioned above, these attributes are not always available. The solution proposed in this work is to use MSAC [30], a variety of RANSAC [31], to detect ground plane G (Eq. (1)). Then, the distances Dpp from the points of cloud P to plan G are calculated (Eq. (2)) and those point within a distance h are discarded as points belonging to the ROI [32]. The threshold distance h is configurable depending on the MLS height. In this work, h is set in 2 m.

$$G = G_A x + G_B y + G_c z + G_D \tag{1}$$

$$Dpp_i = \frac{\left|G_A P_{xi} + G_B P_{yi} + G_C P_{zi} + G_D\right|}{\sqrt{G_A^2 + G_B^2 + G_C^2}} \tag{2}$$

2.4. Sky-coloured points detection

Once the ROI has been delimited, the next step consists of the detection of sky-coloured points. A sample of the sky colour is needed for the correction of the sky-coloured points. The sample S is selected manually in the point cloud P. Although the sky colour may have small variations, a point whose colour matches the original sky must be selected, avoiding sky samples influenced by other elements.

To detect similar colours, the Lab colour space gives better results than the RGB colour space [14,33,34]. Since most image sensors and displays in RGB space correspond to standard RGB (sRGB) space, the colour of the point cloud is considered in sRGB space. The transformation from sRGB to Lab is performed by means of Eq. (3), Eq. (4) and Eq. (5), as indicated in [35]. The illuminant depends on environmental lighting. Since most colour acquisitions are made on sunny days with clear illumination, the illuminant D65 is established by default [36], although it could be changed for other illuminants according to the need of each case study. The RGB colour attributes of the points within the ROI are transformed to the Lab colour space generating the corresponding three new colour attributes P(P_x,P_y,P_z,P_R,P_G,P_B, P_L,P_a,P_b).

$$\begin{pmatrix} P_L \\ P_a \\ P_b \end{pmatrix} = 100 \begin{bmatrix} 0 & 116 & 0 & -16 \\ 500 & -500 & 0 & 0 \\ 0 & 200 & -200 & 0 \end{bmatrix} \begin{pmatrix} f(C_x/C_{xn}) \\ f(C_y/C_{yn}) \\ f(C_z/C_{zn}) \\ 1 \end{pmatrix} \tag{3}$$

where and C_x, C_y and C_z are the tristimulus values of the illuminant (D65 in this case):

$$\begin{pmatrix} C_x \\ C_y \\ C_z \end{pmatrix} = 100 \begin{bmatrix} 0.4124 & 0.3576 & 0.1805 \\ 0.2126 & 0.7151 & 0.0721 \\ 0.0193 & 0.1192 & 0.9505 \end{bmatrix} \begin{pmatrix} P_R \\ P_G \\ P_B \end{pmatrix} \tag{4}$$

$$f(t) = \begin{cases} t^{1/3} & : 1 \geq t \geq 0.008856 \\ 7.787t + (16/116) & : 0 \leq t \leq 0.008856 \end{cases} \tag{5}$$

The colour distances D in channels a and b of the Lab colour space between the sky sample $S = (s_x, s_y, s_z, s_L, s_a, s_b)$ and all points of the ROI are then calculated (Eq. (6)). Not using the L-channel in the distance calculation eliminates the influence of brightness changes. Although the colour of the sky is uniform, in the acquisition of the images brightness and darkening may appear at the transition between sky and object due to the position of the sun. Sky-coloured points are detected as those points with a colour distance Dc_i to the sample S does not exceed a threshold distance d (Eq. (7)) (Fig. 2). The threshold distance d was empirically established in 2000.

$$Dc_i = \sqrt{(P_{ai} - s_a)^2 + (P_{bi} - s_b)^2} \tag{6}$$

$$P_{i\_label}(a, b) = \begin{cases} skyif Dc_i(a, b) < d \\ no\_skyif Dc_i(a, b) > d \end{cases} \tag{7}$$

2.5. Colour reassignment

The sky-coloured points K cannot be restored to their original colour because the original colour has been lost in the colouring process (pixel to point assignment) or original colour has not been acquired correctly in the images. Also, we assume images used for colouring point cloud are no available. To solve this problem, the colour RGB of sky-coloured points K is overwritten by the colour of the no sky-coloured nK nearby points. This is a more realistic solution than leaving the sky-coloured points.

For each sky-coloured point K_i detected in the previous step, its k =

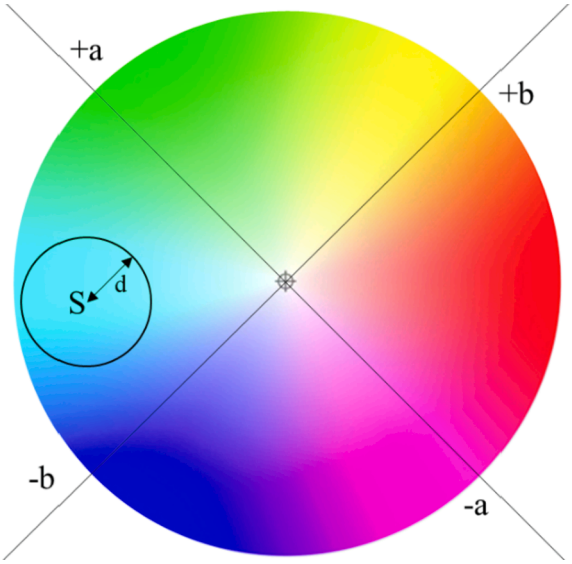

Fig. 2. Lab colour space with sky-colour sample and threshold distance.

25 nearest neighbours [37] are estimated in the no sky-coloured point cloud nK (both within the ROI and outside). The colour distance in the Lab colour space is calculated again from the sky coloured point K_i to the no sky-coloured neighbouring points nK. The RGB colour of the point with the far colour distance (Dn) is selected to overwrite in the RGB attributes of the sky-coloured point. The calculation of the colour distance at this stage allows for less sensitivity to threshold *d* in the sky-coloured point detection. The colour change between sky-coloured points and object-coloured points is gradual, not sharp, and the reassignment based on the larger distance allows for selecting the colour of the object, not the one influenced by the sky-colour yet. In addition, searching for points both inside and outside the ROI allows recover the original colour in false near to the ROI border, since all points outside the ROI keep their original colour.

3. Experiments

3.1. Case studies and equipment

The proposed method was tested in ten real case studies acquired in the surroundings of Palencia (Spain) with a Lynx Mobile Mapper, which integrates a camera Ladybug5 [38]. The case studies were selected for their context in different environments (urban and rural). Two of these case studies did not show colouring errors, so synthetic colouring errors were manually assigned and these case studies with synthetic errors were used to contrast the colours obtained applying the method and the real colours. The remaining eight case studies contained errors in colour assignment by calibration. Case studies 1–4 corresponded to point clouds where vegetation stands out and case studies 5–8 to buildings. These eight case studies present sky-coloured points on various objects. The acquisition was conducted by the morning and the weather was clear (no clouds). The selected sky-coloured sample S corresponds to R = 145, G = 190, B = 230. Colouring errors are clearly visible, especially in trees, where branches and whole sections are sky-coloured. In buildings, sky-coloured areas are centred on cornices, roof edges and borders. Other objects with sky-colour are train chains and streetlights.

3.2. Results on datasets with synthetic errors

The following two case studies were acquired without sky-coloured points, they were used to evaluate the detection of sky-coloured points and especially the re-colouring. Some areas were selected to be manually sky coloured, similar to the errors found in the other datasets. The dataset S1 is mainly composed of two trees, where three zones of the treetop were manually sky coloured. The dataset S2 consists of the building façade, where the cornice, part of the corner of the house and an electric cable were manually sky coloured. Fig. 3 shows the original coloured point clouds, the manually sky-coloured points, and the result of the colour reassignment with the proposed method. The original colour of the point clouds is not recovered, although the areas collected are not easily detectable by a human observer without seeing the point clouds with the sky-coloured points.

The colour reassignment depends on the correct detection of the sky-coloured points and it is analysed quantitatively by means of the metrics *precision* (Eq. (8)), *recall* (Eq. (9)) and *F1-score* (Eq. (10)). The results of the counting True Positives (TP), False Positives (FP), False Negatives (FN), True Negatives (TN) and metrices of each case study are shown in Table 1.

$$precision = \frac{|TP|}{|TP| + |FP|} \tag{8}$$

$$recall = \frac{|TP|}{|TP| + |FN|} \tag{9}$$

$$F1 = 2x\frac{precisionxrecall}{precision + recall} \tag{10}$$

The F1-score is higher in dataset S1, which corresponds to vegetation, than in dataset S2, although dataset S1 also contained a greater number of sky-coloured points. In both datasets, the comparison between *precision* and *recall* shows that the algorithm tends to over-detection. This behaviour is considered better for the sky-coloured points detection than the under-detection. The over-detection minimizes the permanence of sky-coloured points that in the subsequent process of colour reassignment would mean a re-colouring with blue tones of the sky. Also isolated points coinciding with the sky colour were located outside the areas manually coloured, mainly on the façade of the dataset S2. The number of these false detections had a negative influence on the calculation of the *precision*, but their dispersion and mixture between well-coloured points meant that no changes were seen in the visualization of the corrected point cloud with respect to the original data (Fig. 3.d and Fig. 3.f).

In order to quantify the differences in the recoloured with respect to the original, differences were sought between the original point cloud colour and the recoloured result. These colour changes are indicative of detected sky-coloured points. Subsequently, the distance between intensity values of each RGB channel of the recoloured points and the original points was calculated. Table 2 shows the mean, standard deviation, and maximum distance in both datasets with synthetic sky-coloured points. RGB channels have a range of 0–255. The distances are greater in synthetical dataset 1, which corresponds to the trees, than in dataset 2. But both average values of colour distance are very low, less than 2.114 intensity values in the worst scenario. This value is indicative of the proximity of the colour's reassignment by the method to correctly acquired original colours. Fig. 4 compares the histograms of each channel RGB of the recoloured points and the original ones. Although there were small punctual peaks, the curves in each histogram show a very similar distribution between the original and the recoloured points. Only small deviations were located in the dataset S2 between values 67 and 91 of the channel R and between values 103 and 163 of the G channel.

3.3. Results on datasets without synthetic errors: sky-coloured points detection

In Table 3, the detections of the sky-coloured points were counted in case studies without synthetic errors, and the *precision, recall,* and *F1-score* metrics were calculated. The F1-score is 8.9% in those datasets containing mostly vegetation (case studies 1 to 4) than in those

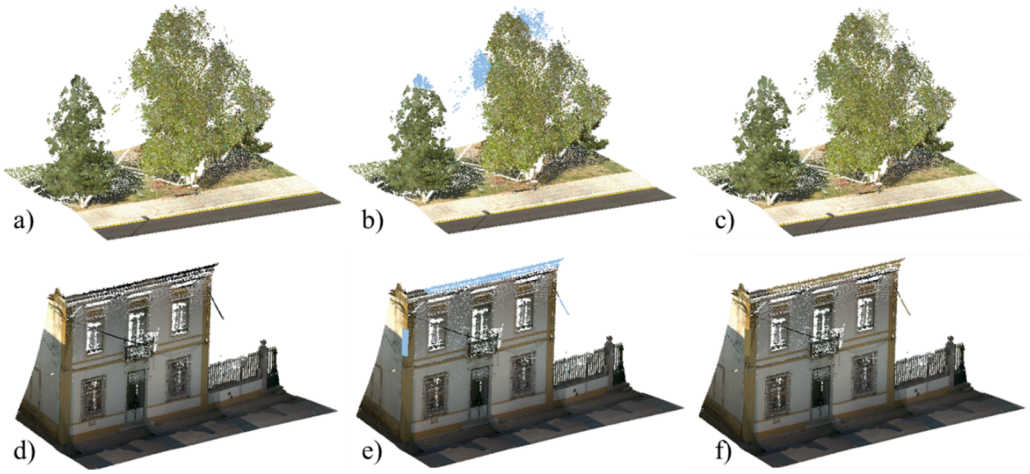

Fig. 3. Cases studies with synthetic errors and results: a) original case study S1, b) synthetic sky-coloured points, c) case study S1 with colour reassignment, d) original case study S2, e) synthetic sky-coloured points, f) case study S2 with colour reassignment.

Table 1
Statistical analysis of each case study with synthetic sky-coloured points.

Datasets	TP (points)	TN (points)	FP (points)	FN (points)	*Precision*	*Recall*	*F1*
Dataset S1	3,233	170,867	374	0	0.896	1.000	0.945
Dataset S2	2,283	781,442	1,284	0	0.640	1.000	0.781
TOTAL	**5,516**	**952,309**	**1,658**	**0**	**0.769**	**1.000**	**0.869**

Table 2
Mean, standard deviation and maximum distance between the recoloured points by the algorithm and the originals per colour channel.

	Channel Red			Channel Green			Channel Blue			All channels		
	mean	std	max	mean	std	max	mean	std	max	mean	std	max
Dataset S1	1.640	1.880	25	1.852	2.415	24	2.114	3.292	25	1.869	2.529	24.6
Dataset S2	0.645	0.894	15	0.655	0.836	14	0.684	0.877	15	0.661	0.869	14.6
TOTAL	**0.926**	**1.212**	**18.7**	**0.968**	**1.242**	**17.6**	**1.034**	**1.385**	**18.8**	**0.976**	**1.280**	**18.4**

containing mostly buildings (case studies 5 to 8). In addition, the datasets with vegetation have a greater number of sky-coloured points. The comparison between *precision* and *recall* shows that the algorithm tends to over-detection, as in datasets with synthetic errors.

3.4. Results on datasets without synthetic errors: Colour reassignment

Figs. 5 and 6 compare the acquired clouds coloured before and after the application of the method. As can be seen, the algorithm correctly detects the sky-coloured points and assigns them the colour of the closest points. Depending on each object, the result presents variations in colour and texture reassigned, which are related to the geometry and colour of the nearest no sky-coloured points.

The most significant results of our method can be seen in the trees because trees initially had more colouring errors (Fig. 5). The sky-coloured points were re-coloured according to the colour of the treetop and without appreciating the difference with the expected original. The reassigned texture also corresponded to the expected original. In addition, the irregular colour patterns with a granular effect of the re-coloured points remain realistic and in line with the rest of the tree. The maintenance of the irregular colour pattern is caused by the irregular distribution of the tree points. In the search for points by proximity, the irregular distribution produces greater variations in the selection of the closest points, and therefore greater variation in the selection of the colour to be re-coloured.

The train chain and the cables of electricity and telephone were also re-coloured correctly (Fig. 5). In their case, the cables were interspersed sky-coloured and original-colour (black) areas, so the reassignment was done on black colour. In addition, as the cables are linear, there were no clear texture and pattern, both in sky-coloured or original-coloured parts.

Buildings were sky-coloured on their cornices and adjacent corners with the sky in the images. Sky- coloured areas often corresponded to high areas with low density of points, given the distance and angle to the MMS. Given the distance to the MMS and the low point density, no colour pattern can be seen in the buildings, either because buildings are painted in solid colour or their patterns are too small to be visible in point clouds. For these reasons, the colour was re-assigned as the solid colour of the closest points and there were no variations as in the vegetation. In buildings, the colour reassignment was done correctly with respect to the nearby points in colour, texture, and patterns (Fig. 6). The colour of the re-coloured building point clouds is more realistic, however real colours cannot be the same as the re-assigned ones, since buildings have abrupt changes in colour, often related to their geometry and semantics.

The upper part of some streetlights in the case studies 4 and 7 (Fig. 7) were sky-coloured, while their lower part was coloured with the background. After applying the method, the areas corresponding to the sky colour were re-coloured with the areas corresponding to the background existing in the lowest part. Although the behaviour of the algorithm was correct and the sky-colour was eliminated in streetlights, the new colour did not correspond to the real streetlights colour.

The proposed method was codified using Matlab and the case studies were processed on a computer with CPU i7-7700HQ 2.8Ghz and 16 GB

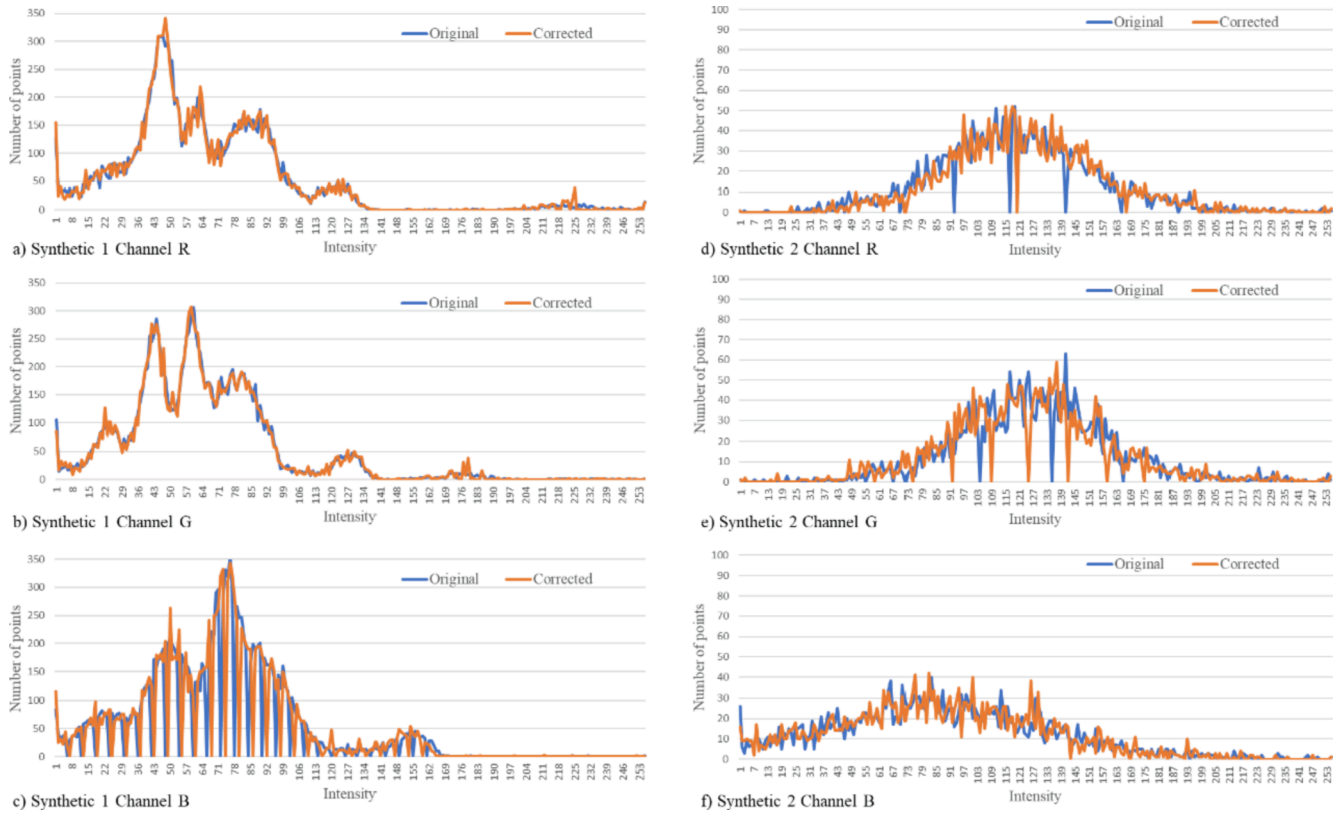

Fig. 4. Comparative histograms of detected sky-coloured points and the original points in case studies with synthetic sky-coloured points.

Table 3
Statistical analysis of each case study.

Datasets	TP (points)	TN (points)	FP (points)	FN (points)	*Precision*	*Recall*	*F1*
1	104,420	1,106,197	7,274	0	0.935	1.000	0.966
2	171,825	1,138,922	990	6,533	0.994	0.963	0.979
3	140,970	1,433,118	7,259	1,417	0.951	0.990	0.970
4	14,899	1,424,695	1,922	0	0.886	1.000	0.939
Vegetation datasets	**432,114**	**5,102,932**	**17,445**	**7,950**	**0.961**	**0.982**	**0.971**
5	113,738	102,255	28,397	274	0.800	0.998	0.888
6	16,129	2,432,418	3,017	242	0.842	0.985	0.908
7	17,639	1,778,647	7,941	0	0.690	1.000	0.816
8	3,313	261,498	392	0	0.894	1.000	0.944
Building datasets	**150,819**	**4,574,818**	**39,747**	**516**	**0.791**	**0.997**	**0.882**
TOTAL	**582,933**	**9,677,750**	**57,192**	**8,466**	**0.911**	**0.986**	**0.947**

RAM DDR4. The processing times, the number of points in each case study are compiled in Table 4. In the processing time, the number of points detected as sky-coloured is more relevant than the total number of points, since it implies in the colour reassignment phase a greater number of points for which to search for neighbours. The processing times are fast, especially in comparison with re-colouring the point clouds (if we still had the images used to colour the point cloud) and much more than making a new acquisition with MMS.

4. Discussion

The designed method was applied to all the case studies with the same values in the sky-sample and the same threshold *d*, showing a very robust behaviour and obtaining an improvement in the colouring in spite of the geometric differences between the objects and the environment. A survey of the point clouds showed that calibration errors are more relevant in vegetation, while constructed elements (buildings or objects) have fewer sky-coloured points. In the case of buildings, the sky-coloured points only were concentrated on cornices. In the case of objects, sky-coloured points focus on those with a single linear geometry (lampposts and cables) or composed by multiple linear geometries (antennas). The objects were the most difficult elements to recover the original colour, because if the majority of the object shares the same geometry that causes the initial colouring error, there are no original colours to reassign the correct colour. However, the differences in geometry helped to maintain the colour patterns in the re-assignment, on both scattered, planar, and linear surfaces. A common behaviour in all the datasets, to a greater or lesser extent, is over-detection, which quantitatively impaired the results of the urban datasets, although visually there are no anomalies in the reassignment of colour, although prioritizing over- versus under-detection enhances colour reassignment.

The position of the sun influences the initial colouring of the point clouds and the proposed method amplifies contrasts in colour. Analysing the shadow projections of existing objects on the environment, the acquisitions of the case studies were made in the morning. The inclination of the sun influences the initial colouring of the point cloud as the images are taken against and in favour of sunlight. This effect can be seen in case studies 1 and 2 (Fig. 5b to d), where the same type of tree (birch)

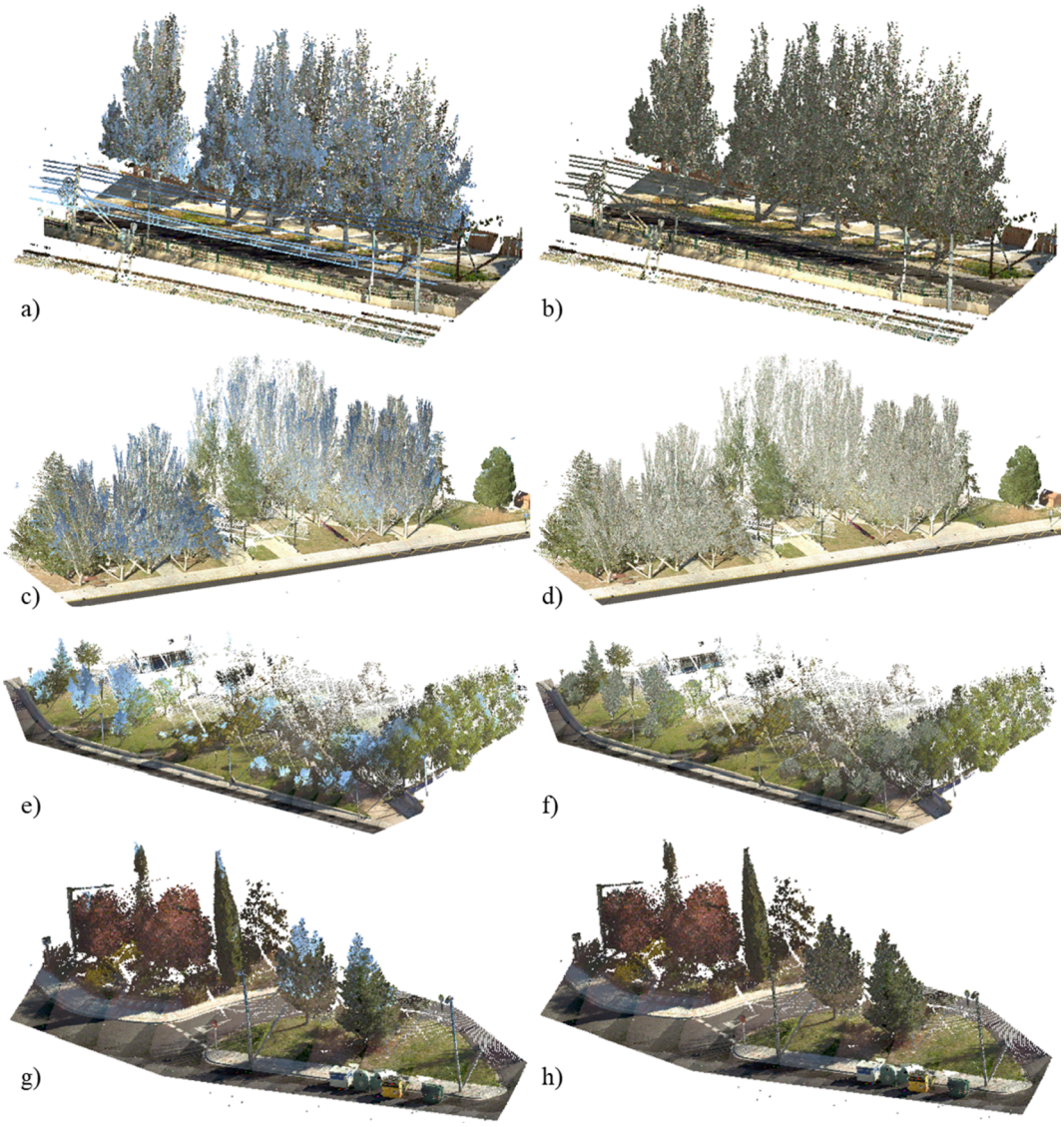

Fig. 5. Case studies 1 to 4 order in rows with sky-coloured points (left) and after applying the colour reassignment method (right). Note: sky-coloured points are those blue points located in the treetops.

was coloured with two colour tones, one darker and one lighter. In the case study 1, the photographs of the trees were taken in backlight, therefore the points closest to the sky-coloured points were darkened points. In the reassignment, the colour of the trees is darker. On the other hand, in the case study 2, the photographs of the trees were taken in light, so there were no dark contrasts between sky and tree point colours and the reassignment colour on trees was more realistic. The times presented in this work correspond to the central daylight hours, when illumination is most constant and most acquisitions with color information are performed. However, acquisitions at different hours will produce different illumination, so it will be necessary to select a new sky color sample and to study the optimum color distance d under different conditions. These tests will be conducted in future work.

The most influential parameter in the method was the assignment of the distance d. The value of $d = 2000$ was set experimentally according to a visual evaluation of the results and it was the same value to process all case studies. In the Fig. 8, results of different values of d in buildings and trees are collected. A low value in d implies that sky-coloured points are preserved, and the reassignment uses the blue colour of the no detected sky-coloured points. A high value in d implies an over-detection of sky-coloured points, mainly points with light colours. Although in the work d has been set at 2000, the Fig. 8 shows that there is very little variation in the results when $d = 2500$. Therefore, d is a robust parameter once all sky-coloured are detected, and d value can be common to analyse different case studies (both vegetation and buildings).

The proposed method has a clear limitation, the false detection as sky-coloured points of those colours that coincide with the sky-colour. In these case studies, the sky colour was matched to blue, therefore blue points in the ROI of buildings, objects and trees were reassigned another colour. Polished surfaces, such as crystals, that although they are not blue, they reflect the colour of the sky. The window glass reflected the sky-colour and is acquired by the photographs. The algorithm detected the sky-coloured points and reassigned to the colour of the nearest points (Fig. 9). Fortunately, blue colour does not predominate in the environment, but even so, the blue colour without the ROI (near ground) were preserved correctly. In case study 4 (Fig. 5g and h), and in case study 8 (Fig. 6g and h), the colour of a blue container and a shop sign were preserved, respectively.

The performance of MSAC for ROI detection was robust and correct in all case studies. Given the distribution of points in the MLS point clouds, which are concentrated along the road in the acquisition trajectory, it is easy for the algorithm to detect the ground plane.

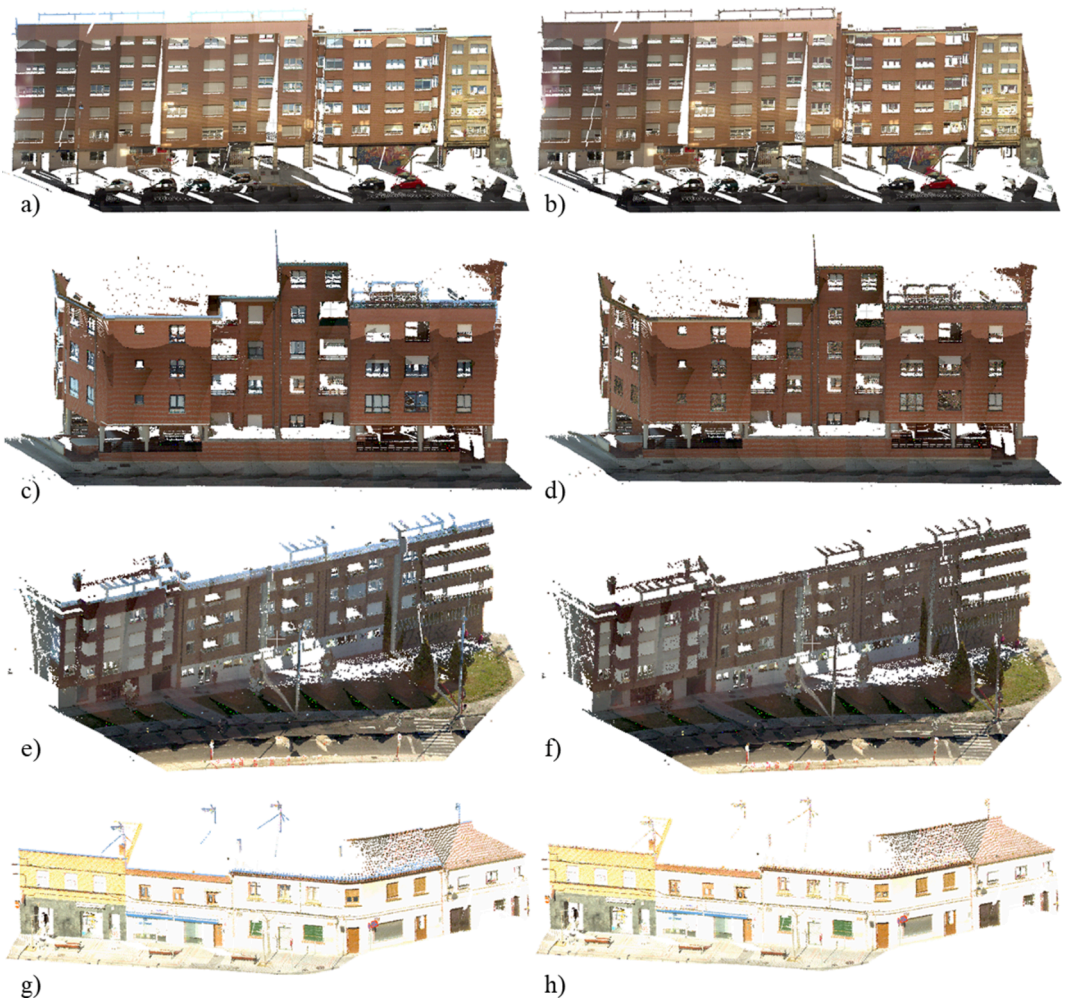

Fig. 6. Case studies 5 to 8 order in rows with sky-coloured points (left) and after applying the colour reassignment method (right). Note: sky-coloured points are those blue points located on the balconies, roofs, and antennas.

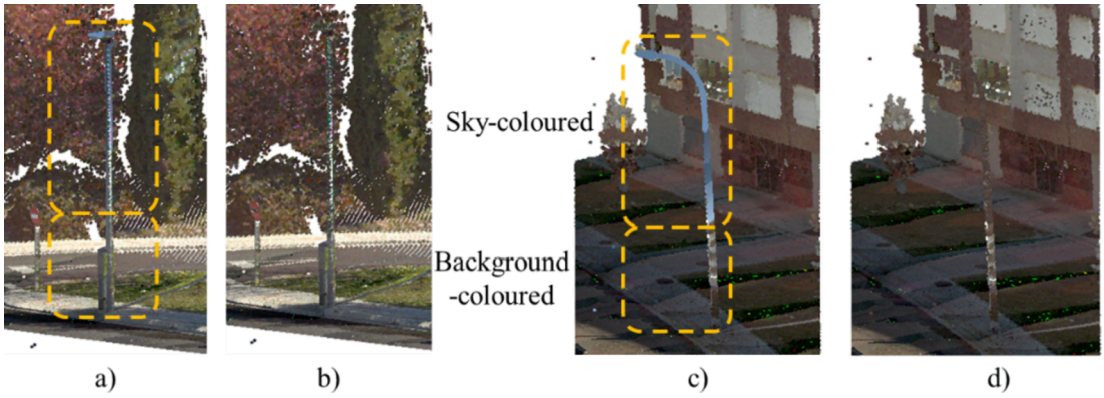

Fig. 7. Application of the method on the streetlights: a) Coloured streetlight in case study 4, b) Recoloured streetlight in case study 4, c) Coloured streetlight in case study 7, d) Recoloured streetlight in case study 7.

Furthermore, since the ROI is related to the height *h* of the MLS, small deviations in plane detection, or small non-flat surfaces are omitted. In case of the existence of road environments with non-flat areas, the point cloud should be preprocessed to segment the MLS point cloud linearly along the road until flat regions are obtained. This can be done by studying the inclination of the road points or by using the trajectory data. In more complex environments, such as those with multiple ground at different heights, the MSAC algorithm detects the ground (road), on which the acquisition was conducted as it contains the most points. Depending on the Z coordinate, the remaining ground points can be part of the ROI where points sky-coloured are detected, in case these multiple grounds exceed the MLS height *h*.

5. Conclusion

This work presents a method based on point cloud processing and

Table 4
Processing times and number of points by case study.

Case Study	Number of points	Points detected as sky-coloured	Processing time
1	1,217,891	111,694	7.3 s
2	1,318,270	172,815	18.1 s
3	1,582,764	148,229	9.5 s
4	1,441,516	16,821	6.2 s
5	2,444,664	142,135	13.6 s
6	2,451,806	19,146	14.7 s
7	1,804,227	25,580	8.9 s
8	257,474	3,705	2.3 s

image processing techniques to correct the existence of sky-coloured points on MLS point clouds produced by an erroneous calibration of the camera. The input data is a coloured point cloud, without other information, such as the images used previously to colour the point cloud, point attributes, and acquisition trajectory, as this data is often not available. The method compares a sample of sky-colour with the remaining point colours of the point cloud in Lab colour space to detect sky-coloured points. Then, the detected sky-coloured points are replaced with the colour of the neighbouring points. The method was tested in ten real case studies, with different types of trees, buildings, and urban objects. Trees are the elements where the colouring errors are most visible, covering a large part of the treetops, while in buildings the sky-coloured points are concentrated on cornices. The algorithm for sky-coloured points detection tends to over-detection and obtained an average *F1-score* of 94.7%, which ensures the correct identification of most of the coloured points as sky. Although it was not possible to recover the original colour of the environment, the point cloud recoloured by the proposed method shows a more realistic alternative than leaving sky-coloured points and improves visualization. The re-coloured areas show realistic colours, textures, and patterns according to the illumination and the geometry. In addition, the image histograms between recoloured and original points are very similar, being the average colour distance between them only 0.976 ± 1.280 intensity levels, which indicates very close colours between the real and the reassigned coloured point cloud. The processing times are shorter than re-colouring the point clouds (if the images were available) or re-acquiring case studies.

Future work will focus on replacing this method with the use of Artificial Intelligence, combining the extraction of diverse geometric features with the colour features to improve the detection of sky-coloured points, the automatic detection of the sky colour without a sample, and an end-to-end application with a Convolutional Neural Network to detect and reassign the correct colours. Another objective in colour correction will be to remove shadows from objects in the point clouds, in order to obtain diffuse lighting. Finally, Neural Networks will be trained with coloured point clouds before and after the colour correction and the results will be contrasted.

CRediT authorship contribution statement

Elena González: Conceptualization, Methodology, Formal analysis, Investigation, Writing – original draft, Writing – review & editing, Visualization, Supervision. **Jesús Balado:** Conceptualization, Methodology, Software, Validation, Formal analysis, Investigation, Writing – original draft, Writing – review & editing, Visualization. **Pedro Arias:** Formal analysis, Investigation, Resources, Writing – review & editing, Visualization, Supervision, Project administration, Funding acquisition. **Henrique Lorenzo:** Resources, Writing – review & editing, Supervision, Project administration, Funding acquisition.

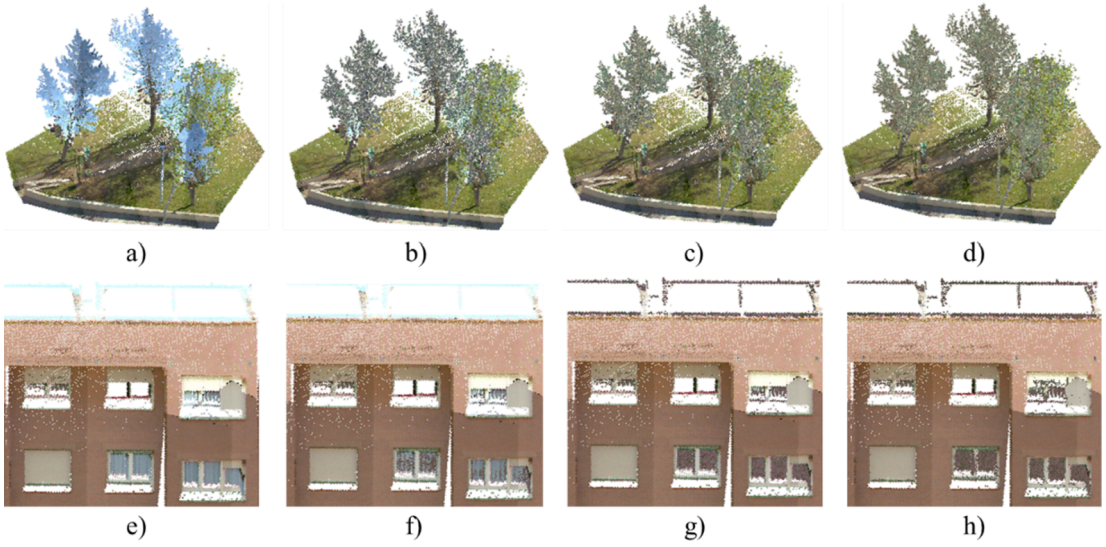

Fig. 8. Comparison and application of the method in partial case studies 3 and 5 (a,e) with d = 1500 (b,f), d = 2000 (c,g) and d = 2500 (d,h).

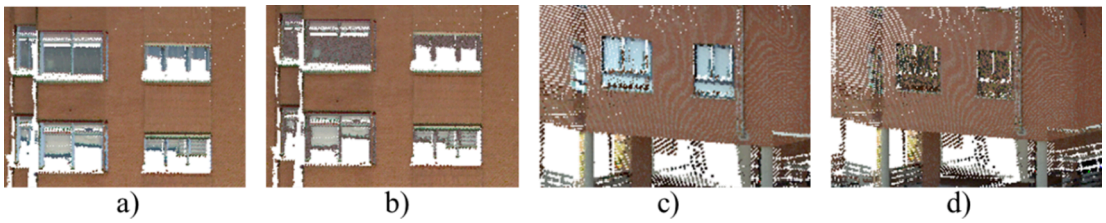

Fig. 9. Expanded case study 5 (a) and 6 (c). Windows detected with sky-colour due to a reflection and re-coloured (b,d).

Declaration of Competing Interest

The authors declare that they have no known competing financial interests or personal relationships that could have appeared to influence the work reported in this paper.

Acknowledgements

Authors would like to thank the Xunta de Galicia given through human resources grant (ED481B-2019-061) and competitive reference groups (ED431C 2020/01). This project has received funding from the Ministerio de Ciencia e Innovación - Agencia Estatal de Investigación/ 10.13039/501100011033 (Proyecto PID2019-105221RB-C43, PID2019-108816RB-I00) and from the European Union's Horizon 2020 research and innovation programme under grant agreement No 769255. This document reflects only the views of the author(s). Neither the Innovation and Networks Executive Agency (INEA) or the European Commission are in any way responsible for any use that may be made of the information it contains. The statements made herein are solely the responsibility of the authors. Funding for open access charge: Universidade de Vigo/CISUG.

References

[1] B. Riveiro, H. González-Jorge, J. Martínez-Sánchez, L. Díaz-Vilariño, P. Arias, Automatic detection of zebra crossings from mobile LiDAR data, Optics and Laser Technology. 70 (2015) 63–70, https://doi.org/10.1016/j.optlastec.2015.01.011.
[2] J. Balado, L. Díaz-Vilariño, P. Arias, H. González-Jorge, Automatic classification of urban ground elements from mobile laser scanning data, Automation in Construction. 86 (2018) 226–239, https://doi.org/10.1016/j.autcon.2017.09.004.
[3] L. Deng, M. Yang, Z. Liang, Y. He, C. Wang, Fusing geometrical and visual information via superpoints for the semantic segmentation of 3D road scenes, Tsinghua Science and Technology. 25 (4) (2020) 498–507, https://doi.org/10.26599/TST.2019.9010038.
[4] E. Grilli, F. Menna, F. Remondino, A review of point clouds segmentation and classification algorithims, ISPRS - International Archives of the Photogrammetry, Remote Sensing and Spatial, Information Sciences. XLII-2/W3 (2017) 339–344, https://doi.org/10.5194/isprs-archives-XLII-2-W3-339-2017.
[5] E. Che, J. Jung, M. Olsen, Object Recognition, Segmentation, and Classification of Mobile Laser Scanning Point Clouds: A State of the Art Review, Sensors. 19 (4) (2019) 810, https://doi.org/10.3390/s19040810.
[6] M. Chen, Y. Tang, X. Zou, K. Huang, L. Li, Y. He, High-accuracy multi-camera reconstruction enhanced by adaptive point cloud correction algorithm, Optics and Lasers in Engineering. 122 (2019) 170–183, https://doi.org/10.1016/j.optlaseng.2019.06.011.
[7] H. Luo, C. Wang, C. Wen, Z. Cai, Z. Chen, H. Wang, Y. Yu, J. Li, Patch-Based Semantic Labeling of Road Scene Using Colorized Mobile LiDAR Point Clouds, IEEE Transactions on Intelligent Transportation Systems. 17 (5) (2016) 1286–1297, https://doi.org/10.1109/TITS.2015.2499196.
[8] X. Kang, J. Li, X. Fan, Line Feature Extraction from RGB Laser Point Cloud, in: 2018 11th International Congress on Image and Signal Processing, BioMedical Engineering and Informatics (CISP-BMEI), 2018: pp. 1–5. Doi: 10.1109/CISP-BMEI.2018.8633181.
[9] J. Strom, A. Richardson, E. Olson, Graph-based segmentation for colored 3D laser point clouds, in, IEEE/RSJ International Conference on Intelligent Robots and Systems 2010 (2010) 2131–2136, https://doi.org/10.1109/IROS.2010.5650459.
[10] Z. Ximin, W. Wanggen, Six dimensional clustering segmentation of color point cloud, in: in: 2016 International Conference on Audio, Language and Image Processing (ICALIP), 2016, pp. 423–427, https://doi.org/10.1109/ICALIP.2016.7846670.
[11] Q. Zhan, Y. Liang, Y. Xiao, Color-based segmentation of point clouds, ISPRS Laser Scanning Workshop. 38 (2009) 248.
[12] K. Sareen, G. Knopf, R. Canas, Rapid clustering of colorized 3D point cloud data for reconstructing building interiors, 2010. Doi: 10.1109/ISOT.2010.5687331.
[13] L. Perdomo, D. Pittol, M. Mantelli, R. Maffei, M. Kolberg, E. Prestes, c-M2DP: A Fast Point Cloud Descriptor with Color Information to Perform Loop Closure Detection, in: in: 2019 IEEE 15th International Conference on Automation Science and Engineering (CASE), 2019, pp. 1145–1150, https://doi.org/10.1109/COASE.2019.8842896.
[14] F. Tombari, S. Salti, L. Di Stefano, A combined texture-shape descriptor for enhanced 3D feature matching, in: in: 2011 18th IEEE International Conference on Image Processing, 2011, pp. 809–812, https://doi.org/10.1109/ICIP.2011.6116679.
[15] L. Huang, F. Da, S. Gai, Research on multi-camera calibration and point cloud correction method based on three-dimensional calibration object, Optics and Lasers in Engineering. 115 (2019) 32–41, https://doi.org/10.1016/j.optlaseng.2018.11.005.
[16] S. Hasan, J. Jansa, N. Pfeifer, BRDF-based correction of colorized aerial LiDAR point clouds (2015), https://doi.org/10.1109/JURSE.2015.7120471.
[17] U. Yilmaz, O. Hellwich, Rapid radiometric enhancement of colored 3D point clouds using color balacing, in: 2010 3DTV-Conference: The True Vision - Capture, Transmission and Display of 3D Video, 2010: pp. 1–4. Doi: 10.1109/3DTV.2010.5506206.
[18] C. Bohak, M. Slemenik, J. Kordež, M. Marolt, Aerial LiDAR Data Augmentation for Direct Point-Cloud Visualisation, Sensors. 20 (7) (2020) 2089, https://doi.org/10.3390/s20072089.
[19] C. Wen, Y. Dai, Y. Xia, Y. Lian, J. Tan, C. Wang, J. Li, Toward Efficient 3-D Colored Mapping in GPS-/GNSS-Denied Environments, IEEE Geoscience and Remote Sensing Letters. 17 (1) (2020) 147–151, https://doi.org/10.1109/LGRS.2019.2916844.
[20] P. Vechersky, M. Cox, P. Borges, T. Lowe, Colourising Point Clouds Using Independent Cameras, IEEE Robot. Autom. Lett. 3 (4) (2018) 3575–3582.
[21] J. Nie, Y. Hu, Z. Ma, Q. Li, Online Colored Point Cloud Acquisition by Reprojection, in, Second International Conference on Intelligent System Design and Engineering Application 2012 (2012) 648–652, https://doi.org/10.1109/ISdea.2012.405.
[22] J. Liu, S. Dai, X. Li, PCCN:POINT Cloud Colorization Network, in, IEEE International Conference on Image Processing (ICIP) 2019 (2019) 3716–3720, https://doi.org/10.1109/ICIP.2019.8803633.
[23] H. González-Jorge, I. Puente, B. Riveiro, J. Martínez-Sánchez, P. Arias, Automatic segmentation of road overpasses and detection of mortar efflorescence using mobile LiDAR data, Optics & Laser Technology. 54 (2013) 353–361, https://doi.org/10.1016/j.optlastec.2013.06.023.
[24] J. Balado, E. González, P. Arias, D. Castro, Novel Approach to Automatic Traffic Sign Inventory Based on Mobile Mapping System Data and Deep Learning, Remote Sensing. 12 (3) (2020) 442, https://doi.org/10.3390/rs12030442.
[25] Y. Mori, K. Kohira, H. Masuda, Classification of pole-like objects using point clouds and images captured by mobile mapping systems, ISPRS - International Archives of the Photogrammetry, Remote Sensing and Spatial Information Sciences. XLII–2 (2018) 731–738. Doi: 10.5194/isprs-archives-XLII-2-731-2018.
[26] M. Soilán, B. Riveiro, J. Martínez-Sánchez, P. Arias, Traffic sign detection in MLS acquired point clouds for geometric and image-based semantic inventory, ISPRS Journal of Photogrammetry and Remote Sensing. 114 (2016) 92–101, https://doi.org/10.1016/j.isprsjprs.2016.01.019.
[27] M. Zhong, L. Sui, Z. Wang, X. Yang, C. Zhang, N. Chen, Recovering Missing Trajectory Data for Mobile Laser Scanning Systems, Remote Sensing. 12 (6) (2020) 899, https://doi.org/10.3390/rs12060899.
[28] B. Lv, H. Xu, J. Wu, Y. Tian, S. Tian, S. Feng, Revolution and rotation-based method for roadside LiDAR data integration, Optics & Laser Technology. 119 (2019) 105571, https://doi.org/10.1016/j.optlastec.2019.105571.
[29] L. Díaz-Vilariño, H. González-Jorge, M. Bueno, P. Arias, I. Puente, Automatic classification of urban pavements using mobile LiDAR data and roughness descriptors, Construction and Building Materials. 102 (2016) 208–215, https://doi.org/10.1016/j.conbuildmat.2015.10.199.
[30] P.H.S. Torr, A. Zisserman, MLESAC: A New Robust Estimator with Application to Estimating Image Geometry, Computer Vision and Image Understanding. 78 (1) (2000) 138–156, https://doi.org/10.1006/cviu.1999.0832.
[31] C. Sahin, Planar segmentation of indoor terrestrial laser scanning point clouds via distance function from a point to a plane, Optics and Lasers in Engineering. 64 (2015) 23–31, https://doi.org/10.1016/j.optlaseng.2014.07.007.
[32] J. Balado, L. Díaz-Vilariño, P. Arias, I. Garrido, Point Clouds To Indoor / Outdoor Accessibility Diagnosis, ISPRS Annals of the Photogrammetry, Remote Sensing and Spatial Information Sciences; ISPRS Geospatial Week 2017. IV-2/W4 (2017) 18–22. Doi: doi.org/10.5194/isprs-annals-IV-2-W4-287-2017.
[33] R. Bello-Cerezo, F. Bianconi, A. Fernández, E. González, F. Di Maria, Experimental comparison of color spaces for material classification, Journal of Electronic Imaging. 25 (2016) 1–10, https://doi.org/10.1117/1.JEI.25.6.061406.
[34] F. Bianconi, R. Bello, A. Fernández, E. González, On Comparing Colour Spaces From a Performance Perspective: Application to Automated Classification of Polished Natural Stones BT - New Trends in Image Analysis and Processing – ICIAP 2015 Workshops, in: V. Murino, E. Puppo, D. Sona, M. Cristani, C. Sansone (Eds.), Springer International Publishing, Cham, 2015, pp. 71–78.
[35] F. Bianconi, A. Fernández, E. González, D. Caride, A. Calviño, Rotation-invariant colour texture classification through multilayer CCR, Pattern Recognition Letters. 30 (8) (2009) 765–773, https://doi.org/10.1016/j.patrec.2009.02.006.
[36] H.R. Kang, Computational Color Technology (2006).
[37] M. Weinmann, S. Urban, S. Hinz, B. Jutzi, C. Mallet, Distinctive 2D and 3D features for automated large-scale scene analysis in urban areas, Computers & Graphics. 49 (2015) 47–57, https://doi.org/10.1016/j.cag.2015.01.006.
[38] I. Puente, H. González-Jorge, J. Martínez-Sánchez, P. Arias, Review of mobile mapping and surveying technologies, Measurement Journal of the International Measurement Confederation. 46 (7) (2013) 2127–2145, https://doi.org/10.1016/j.measurement.2013.03.006.